Geology, biostratigraphy and carbon isotope chemostratigraphy of the Palaeogene fossil-bearing Dakhla sections, southwestern Moroccan Sahara

Mouloud Benammi, Sylvain Adnet, Laurent Marivaux, Johan Yans, Corentin Noiret, Rodolphe Tabuce, Jérôme Surault, Imad El Kati, Sebastien Enault, Lahssen Baidder, et al.

Geology, biostratigraphy and carbon isotope chemostratigraphy of the Paleogene fossil-bearing Dakhla sections, Southwestern Moroccan Sahara

Journal:	*Geological Magazine*
Manuscript ID	GEO-17-1733.R1
Manuscript Type:	Review Article
Date Submitted by the Author:	n/a

Complete List of Authors:	benammi, mouloud; Universite de Poitiers UFR Sciences Fondamentales et Appliquees, Institut de Paléoprimatologie et Paléontologie humaine: Evolution et Paléoenvironnements - iPHEP CNRS UMR 7262 Adnet, Sylvain; Universite de Montpellier, 2Institut des Sciences de l'Evolution de Montpellier (ISE-M), UMR 5554 CNRS/UM/IRD/EPHE Marivaux, Laurent; Universite de Montpellier, 2Institut des Sciences de l'Evolution de Montpellier (ISE-M), UMR 5554 CNRS/UM/IRD/EPHE Yans, Johan; Universite de Namur, Department of Geology Noiret, Corentin; Universite de Namur, Department of Geology Tabuce, rodolphe; Universite de Montpellier, 2Institut des Sciences de l'Evolution de Montpellier (ISE-M), UMR 5554 CNRS/UM/IRD/EPHE Surault, Jerome; Universite de Poitiers UFR Sciences Fondamentales et Appliquees, 1Institut International de Paléoprimatologie, Paléontologie Humaine: Evolution et Paléoenvironnements (iPHEP), UMR-CNRS 7262 El Kati, Imad; Universite Ibn Tofail Kenitra, 5Laboratoire de Géologie, Géophysique, Géorisques et environnement (3GE), Département de Géologie Enault, Sebastien; Universite de Montpellier, Institut des Sciences de l'Evolution de Montpellier (ISE-M), UMR 5554 CNRS/UM/IRD/EPHE Baidder, Lahcen; Universite Hassan II Casablanca, Laboratoire Géosciences Saddiqi, Omar; Universite Hassan II Casablanca, Laboratoire Géosciences Benammi, Mohamed; Universite Ibn Tofail Kenitra, 5Laboratoire de Géologie, Géophysique, Géorisques et environnement (3GE), Département de Géologie

Keywords:	Oligocene, southwestern Morocco, magnetostratigraphy, mammals, chemostratigraphy, biostratigraphy, rodents

Geology, biostratigraphy and carbon isotope chemostratigraphy of the Paleogene fossil-bearing Dakhla sections, Southwestern Moroccan Sahara

BENAMMI MOULOUD[1], ADNET SYLVAIN[2], MARIVAUX LAURENT[2], YANS JOHAN[3], NOIRET CORENTIN[3], TABUCE RODOLPHE[2], SURAULT JÉRÔME[1], EL KATI IMAD[5], ENAULT SÉBASTIEN[2], BAIDDER LAHCEN[4], SADDIQI OMAR[4], BENAMMI MOHAMED[5]

[1]*Institut International de Paléoprimatologie, Paléontologie Humaine: Evolution et Paléoenvironnements (iPHEP), UMR-CNRS 7262, Université de Poitiers UFR SFA, 40 avenue du Recteur Pineau, F-86022 Poitiers cedex, France*

[2]*Institut des Sciences de l'Evolution de Montpellier (ISE-M), UMR 5554 CNRS/UM/IRD/EPHE, CC064, Université de Montpellier, place Eugène Bataillon, F-34095 Montpellier cedex 05, France*

[3]*Department of Geology, University of Namur, rue de Bruxelles 61, 5000 Namur, Belgium*

[4] *Laboratoire Géosciences, Université Hassan II-Casablanca, BP 5366 Maârif, Casablanca, Morocco*

[5]*Laboratoire de Géologie, Géophysique, Géorisques et environnement (3GE), Département de Géologie, Université Ibn Tofail, Faculté des Sciences, BP. 133, Kenitra, Morocco*

ABSTRACT

Recently new Paleogene vertebrate localities were reported in the southern Dakhla area (southwestern Morocco). The Eocene sediment strata crops out on cliffs along the Atlantic Ocean coast. Vertebrate remains come from five conglomeratic sandstone beds and are principally represented by isolated teeth belonging to micromammals, selachians and bony fishes, a proboscidean assigned to ?*Numidotherium* sp., and many remains of archaeocete whales (Basilosauridae). During the fieldwork, five lithostratigraphic sections were described, essentially based on the lithological characteristic of sediments. Despite the lateral variations of facies, correlations between these five sections were possible on the basis of fossil-bearing beds (A1, B1, B2, C1, and C2), and five lithological units were identified. The lower part of the section consists of rhythmically-bedded, chert-rich marine siltstones and marls with thin black phosphorite with organic matter at the base. The overlying units include coarse-grained to microconglomeratic sandstones interbedded with silts, thereby indicating deposition in shallow marine environment with fluvial influence. The natural remanence magnetization of a total of 50 samples was measured, and the intensity of most of the samples is too weak, before or after the first step of demagnetization. The paleomagnetic data of the samples are very unstable, except eight from three similar sandstone levels, which show a normal polarity. Matched with biostratigraphic data on rodents, primates, the selachian, sirenian and cetacean faunas, the new carbon isotope chemostratigraphy on organics 1) refines the age of the uppermost C2 fossil-bearing bed to the earliest Oligocene, and 2) confirms the Priabonian age of the B1 to C1 levels.

Keywords: Oligocene, southwestern Morocco, magnetostratigraphy, mammals, chemostratigraphy, biostratigraphy, rodents

1. Introduction

The study area is in south of Morocco, 60 km south the coastal town of Dakhla (Fig. 1). This area forms a part of the Tarfaya-Dakhla Basin. It is the southernmost Atlantic basin of Morocco, and extends from the Mauritania border in the south to the Canary Islands in the north. It stretches over more than 1000 km along the western margin of the Sahara, and covers an area of 170,000 km^2, both on- and off-shore (Davison, 2005; Sachse et al., 2011, 2014). The geological and stratigraphic structures of the basin have been investigated in detail using well and seismic data (Kolonic et al., 2002, Klingelhoefer et al., 2009 and Davison & Dailly, 2010). The Tarfaya-Dakhla Basin is filled by Mesozoic and Cenozoic continental to shallow-marine sediments, which overlie the basement Precambrian and/or Paleozoic rocks.

The study area is located in the southern margin of the Tarfaya-Dakhla Basin, between latitude 22°50' and 24°05' N; a sector between the gulf of Cintra and N'Tireft village (Fig. 1). The escarpment exposes Paleogene to Quaternary sediments, which have recently been notable for their abundant and diverse marine and terrestrial faunas, particularly vertebrates (Adnet et al., 2010, Zouhri et al., 2014, Benammi et al., 2014a, 2014b, Marivaux et al., 2017). Paleontological data are also exploited by commercial fossil dealers and amateur fossil collectors, a situation which then deserves protection by the authorities as a geosite (Saddiqi et al., 2015).

This work, based on lithologic, paleomagnetic, carbon isotope chemostratigraphy and biochronological data, allows us to describe and refine the nature and age of the sedimentological deposits exposed in the Dakhla region, and notably to constrain the dating of its paleontological content (Paleogene faunas).

2. Geological setting

The studied Paleogene succession corresponds to the Samlat Formation (Fm.) of Ratschiller (1967). It is exposed in different areas, notably cliffs along the Atlantic Ocean coast, and have also been recognized in boreholes drillings (Ranke et al., 1982, Davison, 2005) on the continental shelf. There have been few geological studies carried out on these units in the Dakhla area (e.g. Ratschiller 1967; Ortlieb, 1975), which were inappropriately mapped as Mio-Pliocene by Rjimati et al. (2008), and contrary to those devoted to deposits capping the beach cliffs near Dakhla and dated to the Mio-Quaternary period (e.g. Joleaud, 1907; Front Y Sague, 1911; Deperet, 1912; Lecointre 1962, 1966). In the framework of our geological and paleontological program in the early Tertiary of North Africa, since 2013 we have carried out researches in the westernmost part of the Sahara in Morocco, notably on the geological outcrops of the Samlat Formation exposed between Garitas and about 60 km north of the crossroad at the entrance of the Dakhla peninsula (Fig. 1a, b). Recent paleontological studies in this region have yielded vertebrate fossils, which indicate that some of the deposits are late Eocene in age (Adnet et al., 2010; Zouhri et al., 2014). New sedimentological, geochemical and magnetostratigraphic studies were carried out, in order to refine the age of these Paleogene deposits. Between 2013 and 2015, our field research was devoted to prospecting the outcrops, in search of fossil-bearing levels. The escarpment prospected lies between lat. 22°51' to the south and lat. 24° to the north (in some zones the outcrops are covered by modern sand dunes). About 150 km south of Dakhla, the thickness of the outcrops is reduced and is only a few meters above sea level. It is only from Garitas and beyond to the north, that the escarpment exposes Paleogene sediments, which are notable for their abundant and diverse marine vertebrates.

3. Materials and methods

In order to reconstruct the past sedimentary environment, outcrops were sought in the Dakhla peninsula and in the surrounding areas. For each outcrop, a number of sections were selected for detailed study along the coastal cliffs. The succession of lithofacies was described from the base to the top of the sequence for each section. The description was essentially based on the lithological characteristic of sediments and the sedimentary structures. This description enabled us to establish correlations between sections based on fossil-bearing levels as previously reported in Adnet et al. (2010).

Field studies included selection of different outcrops with easy access; we measured five stratigraphic sequences, bed by bed, with Jacob Staff. These sections are located about 50 km south of Dakhla. In addition, a paleomagnetic study was carried out along the Porto Rico section (Fig. 1). A total of 29 cores were drilled in the field from 13 distinct levels with a portable gasoline powered drill, and oriented in situ with a magnetic compass. Most sites drilled correspond to the Unit 2 and the lower part of Unit 3 (see below). The lithology sampled includes sandstones, clays and silts.

Carbon isotope analyses were performed on 43 samples (Table 1) of the Porto Rico (Pto) and El Argoub (Arg) sections. Organic matter of the sediments was isolated, following the procedure described in Yans et al. (2010) and refined by Storme et al. (2012). The bulk organic carbon isotope analyses ($\delta^{13}C_{org}$) are based on powdered rock samples of about 1 to 10 g, acidified in 25% HCl solution for two hours in order to remove carbonate. The numerous carbonate-free samples were treated similarly. Soluble salts were removed by repetitive (1-10) centrifuging (4000 revolutions per minute) with deionized water until a neutral sediment was obtained. Finally, residues were dried at 35°C and powdered again. Carbon isotope analysis of organic carbon was performed with an elemental analyzer (Carlo-Erba 1110) connected online to a Thermo Finnigan Delta V Plus masspectrometer at the

University of Erlangen (Germany). Organic $^{13}C/^{12}C$ values are normalized to the international VPDB standard (Vienna Pee Dee Belemnite). Each sample was analyzed 1 to 4 times; accuracy and reproducibility of the analyses were checked by replicate analyses of international standards USGS40 and USGS41. The reproducibility of analyses is within 0.2‰ (1σ). The $CaCO_3$ (%) content of the samples was measured with a Bernard Calcimeter.

4. Description of lithological units

Ratschiller (1967) first reported a precise lithology of Cenozoic deposits in Central and Western Moroccan Sahara, and defined the Izic Formation (Fm.). Ranging from the latest Miocene up to the Pliocene, the transgressive Aaiun Fm. (Laayoun area) supposed as Late Miocene in age, and the Paleogene Samlat Fm. Primarily based on foraminifera, Ratschiller (1967) subdivided the Samlat Fm. in three Members (Mb.) as follows:

- the Morcba Mb., which mainly consists of continental sand deposits with some petrified woods, and that is attributed to the Oligocene.

-Early Miocene despite the lack of age evidence.

- the thick Guerran Mb., which is primarily a marine siliceous chalk, becoming more clastic farther onshore, and dated to the Eocene on the basis of foraminifera;

-the Itgui Mb., which consists principally of marine limestones with flint levels, dated from the Paleocene.

The studied deposits of the Dakhla area formally belong to the Samlat Fm., but considering that the lithology of each Ratschiller's Member was defined further north (near Aauinat Tartar, south of Boujdour), we decided here to use lithological units without reference to the Ratschiller's members.

In the Dakhla region, the escarpment lies between 10 and 60m above the sea level, and forms a west facing cliff, steeping on the upper part but sloping gently at the base. The studied sections are directly along a steep cliff at the Atlantic coast exposed between the Gulf of Cintra and the N'Tireft village (Fig. 1b). The Paleogene formation is overlain by a 1 to 2m thick lumachellic limestone, which is Mio-Pliocene in age (e.g. Joleaud, 1907, Front Y Sague, 1911, Deperet, 1912, Lecointre, 1966), and consists of:

- alternating marine limestones and marls, rich in organic matter at the base;
- alternating sandstones and marls, with intercalations of brown to black siliceous limestones at the middle interval;
- sandy white marls at the top.

4.a. Garitas section

This section is directly exposed along the cliff located about 15 km north of Imlili village, in a locality named Garitas, which is located in a restricted military area. Lateral variations of facies are obvious, especially regarding strata thickness (Fig. 4c). We have divided these sequences into five lithological units (U1-5).

Unit U1:

This unit represents the lowermost part of the section, as in Adnet et al. (2010), and is composed of a succession of four lithofacies (Fig. 2).

1- The first Unit is a rhythmic sequence that consists of gray-beige marl limestone to whitish surface, sometimes siliceous with splintery fracture. This marly limestone, showing sporadic black nodules, alternates with marl gray or blackish rich in organic matter (Fig. 3a-c).The base of this sequence shows a ~10-cm-thick blackish phosphorite with rich organic matter including numerous coprolites and fish remains (level A1, Fig. 3c). This last level becomes thicker (20-cm thick) and whiter toward the south.

2- Alternating beige marl and siliceous limestone with vertical fissure filled with the same sediments (Neptunian dykes; Fig. 3e-f). The limestone beds show inverse graded bedding (decimetric at the bottom and multi-decimetric at the top). Several coprolite levels (Fig. 4a) are noted, with centimeter to decimeter thick.

3- Compact gray limestone bars and beige sandy calcareous marl (Fig. 4b).

4- A landmark level composed of black to brown or dark siliceous limestone, rich in coprolites at its base and alternating with beige marls (Fig. 4b).

Unit U2:

This second unit is composed of two lithofacies.

5- Yellowish sandy marl (≈ 1m) overlaid by a friable sandy micro-conglomeratic ferruginous level, which is particularly rich in selachians teeth and vertebrates bones (bed B1 of Adnet et al., 2010). This fossil-bearing level B1 (Fig. 4c) has yielded a large number of vertebrae of cetaceans belonging to five different species, with possible rib fragments of sirenians, as well as few remains of crocodiles, turtles, sea snakes and birds (Zouhri et al., 2014).

6- Whitish marl level with intercalations of lenticular brown siliceous limestone (≈ 5m) (Figs. 4b and 5a).

Unit U3:

This third unit comprises three lithofacies.

7- Muddy brown yellow sandstone, sometimes with a secondary gypsum element. This level yields abundant remains of selachians and archaeocetes (basilosaurids) (cf. Bed B2 of Adnet et al., 2010). Zouhri et al., (2014) reported from this level a *Basilosaurus* sp. and remains of a dugongid (Fig. 6a, b)

8- Fossil-rich beige sandy marl, yielding few dental remains of terrestrial mammals (rodent incisor) and selachians (Level C1).

9- Beige sandy marls.

Unit U4:

10- Red Sands (≈ 0.5m).

Unit U5:

11- A consolidated coquina deposit with oysters and gastropods (scallops bed (≈1,5m)).

4.b. Porto Rico section

The section is located about 10 km east of the Dakhla city, along the seashore of Porto Rico (Fig. 1b). In this area, the available section starts with the bone-bed fossil-bearing level B1 of U2 (Fig. 7), the U1 being under water (or perhaps absent?). This section consists from the bottom to the top of:

Unit U2:

1- At the seashore edge, the geological section begins with an oxidized sandy marl level, rich in vertebrate bones and selachian teeth, corresponding to level B1 of Adnet et al. (2010) (Fig. 7a). This very fossiliferous horizon lies on the previous section more than 22m above the sea level, and plunges northwardly below the sea level.

2- Beige to whitish sandy marls topped by a yellowish and oxidized sandy marl level that is rich in fossils, fossil-bearing level B2 of Adnet et al. (2010) (Fig. 7c). These levels tend to disappear within a few hundred meters to the north of Porto Rico (see Fig. 11 correlation).

Unit U3:

3- The middle of the section corresponding to the U3 consists of a thick multicolor sandy marl series, interstratified by sandstone with limestone concretions. A rich level of selachian teeth and bones (Level C1), was identified in the lower part of this interval (Fig. 7b).

Unit U4:

4- This Unit begins with a very characteristic landmark level consisting of gastropod and oyster coquina (Fig. 7b and 7d), white sandy marls in the middle, with another fossil-bearing level C2, including sandstone intercalations.

Unit U5:

5- The section ends with the Mio-Pliocene flagstone consisting of a coquina limestone, which includes oyster shells and gastropods (U5).

4.c. North Porto Rico and El Argoub sections

These two sections are characterized by the development of both U3 and U4 units formed mainly by sandy marls, and separated by the landmark gastropod coquina limestone (Fig. 8).The U4 shows green marls containing the fossiliferous level C2 at its base, red mudstones and laminated sandstones in the middle, and white sandy marls at the top. The U5 consists of a flagstone formed by laminated sandy-limestones containing millimetric grains of quartz.

5. Correlation between the sections

The North-South logged sections were correlated based on, at least, five remarkable fossil-bearing levels (noted A1, B1, B2, C1, and C2). In these measured sections, the aforementioned lithostratigraphic units show lateral variations of facies along the coastline

(Fig. 9). These variations can be explained by the slight northward tilting of these deposits. The five units recognized represent a general regressive trend, which records a transition from an outer ramp into a peritidal zone. The rhythmic bedding might have been caused by fluctuations in the depositional environment.

With the exception of U5, the four units U1-4 are Paleogene in age and thus formally belong to the Samlat Fm. (see before). The correlations with the three members of the Samlat Fm. of Rattschiller (1967) remain hypothetical, and suffer from inconsistent observations. Rattschiller (1967: fig. 176) illustrated a beach cliff around Porto Rico, where he considered that the Aaiun Fm. directly overlies the Lebtaina Fm., a formation underlying the Samlat Fm. However, it seems that what he considered as the Aaiun Fm., rather corresponds to the U3-5 of the Dakhla area, and that the Lebtaina Fm. corresponds to U1-2. Indeed, if it was firstly expected to attribute the U1-2 to the Guerran Mb. and the U3-4 to the Morcba Mb. According Rattschiller (1967), we cannot confirm the lithological divisions of Rattchiller (1967).

6. Paleomagnetic analysis

Samples were analyzed with the paleomagnetic facilities housed at the iPHEP of the Université de Poitiers, France. Remanent magnetization was measured with a JR6 magnetometer combined with stepwise thermal or alternating field demagnetization in a magnetically shielded room. To better constrain the magnetic mineralogy, we studied the acquisition of isothermal remanent magnetization (IRM), and then the stepwise thermal demagnetization of three-axis differential IRM following the method of Lowrie (1990). The specimens were subjected to stepwise thermal demagnetization in steps up to 600°C. The IRM was determined with a pulse electromagnet. Thermal demagnetization was done with a magnetic measurement thermal demagnetizer (MMTD80) shielded furnace. Progressive thermal demagnetization was carried out, in steps of 30 to 40°C, from 100°C, until either the magnetization intensity fell below the noise level or the direction became erratic. The majority of specimens were submitted to stepwise alternating field (AF) demagnetization with increments of 5–10 mT, using a Molspin Ltd. high-field shielded demagnetizer. Characteristic magnetization components were isolated by applying the method of Kirschvink (1980) to vector segments with a maximum angular deviation less than 15°.

6.a. Magnetic properties and characteristic directions

A set of rock magnetic experiments was conducted to characterize and identify the magnetic mineralogy of the main lithologies. We first analyzed the acquisition of IRM (Isothermal Remanent Magnetization) up to 500 mT and its subsequent thermal demagnetization. Following the procedure described by Lowrie (1990), magnetic fields of 1, 0.4 and 0.12 T were successively applied to each of the three perpendicular directions prior to thermal demagnetization. The IRM acquisition curves (Fig. 11a) show a broad range of coercivities. The initial increase of magnetization up to 100–150 mT indicates the presence of low coercivity minerals. Saturation was achieved between 300 and 500mT, which indicates the presence of intermediate coercivity minerals.

Thermal demagnetization shows that the low field (0.12 T) component is dominant, in figures 11b,c, the first drop appears on the soft and medium components between 300°C and 350°C, indicating the existence of magnetic mineral with soft coercivity, probably corresponding to low-Tititanomagnetite. The second drop is observed at 580°C indicating the presence of magnetite. The harder components, less than 25% of the total IRM, decrease regularly up to temperature of 300–350°C and suggest the presence of a Fe-sulphide.

Thermomagnetic curves are routinely used in paleomagnetism to identify remanence carriers. Low-field susceptibility measurements (*k*–*T* curves) were performed using a Bartington susceptibility meter (MS-2) equipped with furnace. Some specimens were heated up to 600°C at a heating rate of 10°C·min−1, and then were cooled at the same rate (Fig. 11d). The thermomagnetic behavior of bulk sediment samples shows very low magnetization, in agreement with low intensity of the sample. At about 400°C, magnetization starts to increase, is maximal at about 500°C, and then decreases sharply to 0 just before 600°C. This is due to the presence of pyrite, a paramagnetic mineral that altered towards magnetite near 500°C during the experiment (Strechie et al., 2002; Tudryn & Tucholka, 2004). Cooling curves indicate that magnetite is produced as a result of the thermal breakdown (Fig. 11d). No correct curve was obtained for the majority of samples because of low initial signal of magnetic susceptibility.

The natural remanent magnetization displays moderately high values, starting at 8.8x10^{-7} A/m in siltstone levels, and reaching up to ~ 6.3x10^{-4}, with an average of 1.9x10^{-4}A/m (Fig. 10). After some step demagnetization, the magnetization intensity fell below noise level of the magnetometer (Fig. 12a), and the direction became erratic (Fig. 12b). Data resulting from AF and thermal demagnetization were plotted on orthogonal vector plots (Zijderveld, 1967). To determine characteristic magnetic directions, principal components analysis was carried out on all samples. These paleomagnetic directions were then analyzed, using Fisher statistics, to determine site mean declinations, mean inclinations and associated precision parameters.

Only tree strata at the upper part of the section gives a coherent result of normal direction (Fig. 12c). The mean directions of ChRM are: declination = 324.4°, inclination = 44.6° ($\alpha 95$ =24.4, k =6), and differ from the expected direction for this latitude (I=27.2, D=352.2) (Fig. 12d).

7. Carbon isotope geochemistry results

Carbon isotopic values range from -27.8‰ (sample ARG15-2) to -22.1‰ (sample PTO15-11; Table 1). These data are in good agreement with the expected $\delta^{13}C$ values on organics at the Eocene-Oligocene interval (see Sarkar et al., 2003). Seven samples have Total Organic Carbon too low (<0.01%) to perform reliable isotopic analysis.

In the Porto-Rico section, the $\delta^{13}C_{org}$ curve shows the following successive values/trends, from the base to the top (Fig. 13; Table 1):

1. relatively negative $\delta^{13}C_{org}$ value (-27.6‰) in the B1 fossil-bearing level, at the base of the section (lowermost part of unit U2);
2. relatively stable $\delta^{13}C_{org}$ values (from -25.1 to -24.3‰) in the U2 (including the fossil-bearing B2 level);
3. relatively negative $\delta^{13}C_{org}$ value, around -25.7‰ in the lower part of U3 (including the C1 fossil-bearing level);
4. relatively stable $\delta^{13}C_{org}$ values (from -25.2 to -24.6‰) in the upper part of U3;
5. prominent and rapid positive shift of $\delta^{13}C_{org}$ values, from -26.2‰ to -22.1‰ in the uppermost part of U3 and U4;
6. negative shift of $\delta^{13}C_{org}$ values, from -22.1‰ to -25.4‰ in the lower part of U5 (including the C2 fossil-bearing level);
7. positive shift of $\delta^{13}C_{org}$ values, from -25.4‰ to -23.7‰ in the upper part of U5;
8. negative shift of $\delta^{13}C_{org}$ values, from -23.7‰ to -25.2‰ in the uppermost part of U5.

In the El Argoub section, the $\delta^{13}C_{org}$ curve shows the following successive values/trends, from the base to the top (Fig. 13; Table 1):

1. prominent and rapid positive shift of $\delta^{13}C_{org}$ values, from -27.8‰ to -23.4‰ in the uppermost part of U3 and U4;

2. negative shift of $\delta^{13}C_{org}$ values, from -23.4‰ to -25.7‰ in the lower part of U5 (including the C2 fossil-bearing level);
3. positive shift of $\delta^{13}C_{org}$ values, from -25.7‰ to -23.0‰ in the upper part of U5;
4. negative shift of $\delta^{13}C_{org}$ values, from -23.0‰ to -25.5‰ in the uppermost part of U5.

The $CaCO_3$ contents range from 0.0 to 76.9% in the Porto-Rico section and from 0.0 to 45.3% in the El Argoub section.

8- DISCUSSION

The fossil content of the Dakhla deposits is rich and varied, mixing primarily selachians and marine mammals (cetaceans and sirenians). Ratschiller (1967) first mentioned the occurrence of fish teeth in the Eocene Guerran Mb. of the Samlat Fm. In the Dakhla area, a rich vertebrate fauna was discovered by Adnet et al., (2010) in two levels: B1 and B2. The Eocene age proposed by Ratschiller (1967) and later by Adnet et al. (2010) was based on paleontological evidence. Indeed, the majority of selachian taxa (such as *Xiphodolamia serrata*, *Misrichthys stromeri* and *Cretolamna twiggsensis*) recovered in B1 and B2 are known elsewhere in deposits dating from the Bartonian and Priabonian (e.g. Qasr El Sagha Fm. [Egypt], Qa'Faydat and the Wadi Esh-Shallala Fm. [Jordan], or the Drazinda Shale Mb. of the Kirthar Fm. [Pakistan] (Adnet et al., 2010). Later, Zouhri et al. (2014) described five archaeocete cetacean species from the level B1, and dugongid sirenians in the level B2; faunal correlations with the late Eocene of Egypt indicate a Priabonian age for the B1 and B2 fossil assemblages.

Since 2013, our fieldwork allowed the discovery of new fossil-bearing levels in the stratigraphic sequence (A1, C1, and C2). The lowermost part of the Garitas section (U1; Figs. 2 and 3) has yielded a fossil-bearing level including a diverse assemblage of fish (e.g. *"Carcharias" koerti, Physogaleus* aff. *tertius, Coupatezia* spp. *Merabatis* sp., *Burhnamia* sp., *Cyladrincanthus* sp.). In the Porto Rico section (Fig. 7), two stratigraphically distinct levels have yielded fossil vertebrates. The level C1, located at the base of U3 has yielded an assemblage of selachians (e.g. *Carcharhinus* spp. *Carcharias* sp*., Pristis* cf. *lathami, Pastinachus* sp*., Aetobatis* cf. *irregularis*). Above in the section, the base of U4 has yielded a fossil assemblage (C2) of marine and estuarine invertebrates (lamellibranches) and vertebrates (including fishes, turtles, crocodiles, and selachians resembling to C1), together with terrestrial mammals (including rodents, primates, hyracoids, an elephant shrew, and creodonts). A strictly similar fossil assemblage was found in the El Argoub section, in equivalent deposits (i.e. at the base of U4).

The mammal fossils of C2 (Porto Rico and El Argoub) consist of isolated teeth, but also partial jaws and bone fragments. Among the mammals, afrotherians are illustrated by a herodotiine macroscelid (*Herodotius* aff. *pattersoni*) and several "saghatheriid" hyracoids, among which is a species of *Saghatherium*. Primates include an oligopithecid anthropoid (*Catopithecus* aff. *browni*) and an indeterminate afrotarsiid. Rodents are much more abundant and represented by members of two phylogenetically distinct groups: Hystricognathi and Anomaluroidea. Several tens of isolated teeth of anomaluroids indicate the presence of two distinct families, Anomaluridae and Nonanomaluridae, and possibly the ancestral family Zegdoumyidae, represented by five new species (*Argouburus minutus, Paranomalurus riodeoroensis*, *Dakhlamys ultimus*, *Oromys zenkerellinopsis*, and *Nonanomalurus parvus*; see Marivaux et al. 2017). Regarding hystricognaths (Marivaux et *al.*, *in* press), distinct taxa are recognized, primarily including several "phiomyid"-like representatives (*Birkamys* aff. *korai*, *Mubhammys* sp. nov., ?*Phiocricetomys* sp., *Neophiomys* sp. nov., and a new genus and species) and gaudeamurids (*Gaudeamus* cf. *hylaeus* and *G.*cf. *aslius*). Most of these Dakhla C2 mammals (except anomaluroids; Marivaux et al., 2017), or at least their close relatives, have been originally described from well-known Egyptian localities of the Jebel Qatrani

Formation (Fayum Depression), dating from the latest Eocene (L-41; Hyracoidea: Rasmussen & Gutiérrez 2010; Macroscelididae: Simons et al. 1991; Primates: Simons 1995; Simons & Rasmussen 1996; Seiffert 2012; Rodentia: Sallam et al. 2011; Sallam & Seiffert, 2016) or the early Oligocene (Hyracoidea: Rasmussen & Gutiérrez 2010; Rodentia: Wood, 1968). This faunal similarity thus indicates a latest Eocene-early Oligocene time frame for the fossiliferous concentration of the level C2 of the Pto-Arg sector.

Here we performed new chemostratigraphic investigation using carbon isotopes from dispersed organic matter ($\delta^{13}C_{org}$) on the Porto Rico and El Argoub sections, in order to refine the stratigraphic framework of the Samlat Fm. in the Dakhla area. As mentioned above, Adnet et al. (2010) suggested a Bartonian to Priabonian age for the fossil-bearing levels B1 and B2 on the basis of the selachian fauna. Later, Zouhri et al. (2014) refined the age of the level B1 and proposed early-middle Priabonian on the basis of the cetacean fauna. These authors also suggested a Priabonian age for the level B2 on the basis of the sirenian fauna. It implies that the lower part of the studied sections, containing the levels B1 and B2, is (early-middle) Priabonian in age, thereby suggesting that the upper part of the section is Priabonian or younger.

The Eocene–Oligocene boundary (EOB; ~ 34Ma) is the largest global cooling of the Cenozoic Era and led the Earth's climatic system to change from a greenhouse to an icehouse mode, well documented in marine setting (e.g. Bohaty et al., 2012) and, to a lesser extent in continental setting (e.g. Tramoy et al., 2016). The cooling interval, initiated in the late Eocene, comprise several isotopic events, which have been coded by Miller et al. (1991). The oldest of the events, coded Oi-1 or Eocene-Oligocene (climate) transition or EOT, is associated with major $\delta^{18}O$ and $\delta^{13}C$ positive shifts, starting in the late Eocene and ending in the early Oligocene (e.g. Coxall et al., 2005; Katz et al., 2008; Lear et al., 2008). Using a high-resolution carbon isotope study of the ODP site 1218, Erhardt et al. (2013) showed that the carbon and oxygen positive shifts of the Oi-1 event are followed by two positive $\delta^{13}C$ and $\delta^{18}O$ excursions called Oi-1a and Oi-1b, early Oligocene in age. This isotopic pattern was also observed by Zhifei et al. (2004) in ODP Leg 208 Site 1262, 1265 and 522.

In the Porto Rico (Pto) and El Argoub (Arg) sections (this study; Fig.13), the Oi-1 event initiates in the uppermost part of the U3 lithological unit (~ 2 meters below the C2 level) and ends below the C2 level. This isotopic event is followed by one positive excursion (positive shift followed by a negative shift), interpreted here as Oi-1a. In summary, the C2 level is clearly above the Oi-1, and as such it is probably earliest Oligocene in age.

Lower, the B1 and B2 fossil-bearing levels are dated as Priabonian by the selachian, cetacean and sirenian faunas (see above). The C1 level is located in a negative $\delta^{13}C$ excursion (Fig.13). This latter should correspond to the carbon isotope excursion observed in the Priabonian (NP19-20 Zones). The B1 level shows negative $\delta^{13}C$ value, most probably corresponding to the negative $\delta^{13}C$ values in the early Priabonian NP18 Zone (Fig.13).

The paleomagnetic analysis show that the only normal polarity is represented by tree strata situated 2m above the C1 fossiliferous level. Although the rock magnetic properties suggest that the NRM may be of primary origin, we evaluate other criteria to infer the origin of the observed characteristic remanence. In situ site mean directions differ significantly from the direction of the axial geocentric dipole at the latitude of the site (Fig. 12D) and, therefore, exclude a recent magnetic overprint. Correlation of the Porto Rico section with the geomagnetic polarity time scale (GPTS) of Gradstein et al. (2012) was performed by considering the earliest Oligocene age discussed above for C2 level and Priabonian age for B2 and C1. Taking into account the biochronological age, the normal polarity might then be correlated to ChronC16n.

Our new chemostratigraphic and paleomagnetic data suggest that the C2 fossil-bearing level of Dakhla is clearly located above the Oi-1 event and below the Oi-1a event. The Oi-1 event, bringing the major cooling, is recognized by many authors to occur a few 100 kyr later than the GSSP (Global Boundary Stratotype Section and Point) of the Rupelian (Eocene-Oligocene boundary; Vandenberghe et al., 2012). The GSSP of the Eocene-Oligocene boundary is defined in the Massignano section (Italy), and the key marker of the GSSP is the extinction of the hantkeninid planktonic foraminifera, which lies within nannofossil Zone NP21 (Premoli-Silva & Jenkins, 1993).Katz et al. (2008) showed that 1) the Oi-1 event is located around the transition of Chron C13r and C13n (33.545 Myr), and 2) the Oi-1a event is located around the transition of Chron C13n and C12r. It suggests that the C2 level, located just above the Oi-1 event and below the Oi-1a event, is a few 100 kyr above the Eocene-Oligocene boundary, within the nannofossil Zone NP21and into the magnetic polarity Chron 13n.Interestingly, as mentioned above, Gingerich (1993) suggested that the L-41 level (lower part of the Jbel Qatrani Fm.) is located in the early Oligocene. Underwood et al. (2013) places the base of the Jebel Qatrani Formation close to the base of Chron C13n. On the other hand, Seiffert (2006) concluded that the L-41 of Fayum bed falls within a zone of reverse polarity and correlated with Chron 13r, late Eocene, i.e older than the C2 level of Dakhla. The new rodent assemblage from the earliest Oligocene of Dakhla (Sahara, Morocco), represents therefore the first Oligocene record of rodents from northwestern Saharan Africa, especially from the Atlantic margin of that landmass. The carbon isotope chemostratigraphy confirms that the lower part of the studied sections, containing the levels B1 and B2, is early-middle Priabonian in age.

Our knowledge of the mammal faunas documenting the early Oligocene of Afro-Arabia has so far derived from contemporary localities found in northern Egypt (Fayum Depression), Libya (Zallah Oasis) and Oman (Dhofar Province) (Fejfar, 1987; Sallam et al., 2011, 2016, Coster et al., 2010, 2012, Sallam & Seiffert, 2016). This new earliest Oligocene mammal fauna from the northern Atlantic margin of Africa is of great interest because it documents for the first time the diversity of micomammals, especially rodents. Biochronology and C isotope chemostratigraphy provide an Oligocene age constraint of C2 fossiliferous level, and thus increase our understanding of the timing of mammal evolution and environmental changes in North Africa at that time.

Acknowledgments

We would like to thank Abdallah Tarmidi and Mbarek Fouadasi for their help during the field work. Financial supports during the field work were provided by the French ANR EVAH (ANR-09-BLAN-0238) and ANR-ERC PALASIAFRICA (ANR-08-JCJC-0017) Programs, the ISE-M UMR 5554CNRS/UM/IRD/EPHE, CNRS-CoopIntEER171834, and iPHEP UMR CNRS 7262. C.N. and J.Y thank the project BR/121/A3/PALEURAFRICA of the Belgian Science Policy Office.

REFERENCES CITED

ADNET, S., CAPPETTA, H. & TABUCE, R. 2010. A Middle–Late Eocene vertebrate fauna (marine fish and mammals) from southwestern Morocco; preliminary report: age and palaeobiogeographical implications. *Geological Magazine* **147**, 860–870.

BENAMMI, M., ELKATI, I., ADNET, S., MARIVAUX, L., TABUCE, R., SURAULT, J., BAIDDER, L., SADDIQI, O. & BENAMMI, M. 2014. Corrélation de coupes lithostratigraphiques le long des falaises côtières dans la region d'El Argoub (Dakhla, Maroc): Second North African Vertebrate Palaeontology Congress-NAVEP2, Ouarzazate, Morocco, 1-8 September, Abstracts, p.37.

BENAMMI, M., ELKATI, I., ADNET, S., MARIVAUX, L., TABUCE, R., SURAULT, J., BAIDDER, L., SADDIQI, O. & BENAMMI, M., 2014. Preliminary paleomagnetic data in the Dakhla, Southwestern Moroccan Sahara: Second North African Vertebrate Palaeontology Congress-NAVEP2, Ouarzazate, Morocco, 1-8 September, Abstracts, p.40.

BOHATY, S.M., ZACHOS, J.C. & DELANEY, M.L. 2012. Foraminiferal Mg/Ca evidence for Southern Ocean cooling across the Eocene/Oligocene transition. *Earth and Planetary Science Letters* **317–318**, 251–261.

COSTER, P., BENAMMI, M., LAZZARI, V., BILLET, G., MARTIN, T., SALEM, M., ABOLHASSAN BILAL, A., CHAIMANEE, Y., SCHUSTER, M., VALENTIN, X., BRUNET, M. & JAEGER, J.-J., 2010. *Gaudeamuslavocati* sp. nov. (Rodentia, Hystricognathi) from the lower Oligocene of Zallah, Libya: First African Caviomorph?. *Naturwissenschaften* **97**, 697-70.

COSTER, P., BENAMMI, M., SALEM, M., BILAL AWAD, A., CHAIMANEE, Y., VALENTIN, X., BRUNET M. & JAEGER, J.J., 2012. New hystricognathous rodent from the Early Oligocene of central Libya, (Zallah Oasis, Sahara Desert): systematic, phylogenetic, and biochronologic implications. *Annals of Carnegie Museum* **80**, 239–259.

COXALL, H.K., WILSON, P.A., PÄLIKE, H., LEAR, C.H. & BACKMAN, J. 2005. Rapid stepwise onset of Antarctic glaciation and deeper calcite compensation in the Pacific Ocean. *Nature* **433**, 53–57.

CRAMER, B.S., TOGGWEILER, J.R., WRIGHT, J.D., KATZ, M.E. & MILLER, K.G., 2009. Ocean overturning since the Late Cretaceous: inferences from a new benthic foraminiferal isotope compilation. *Paleoceanography*, published online 23 December 2009.doi:10.1029/2008PA001683.

DAVISON, I. 2005. Central Atlantic margin basins of North West Africa: geology and hydrocarbon potential (Morocco to Guinea). *Journal of African Earth Sciences* **43** (1-3), 254–274.

DAVISON, I. & DAILLY, P. 2010. Salt tectonics in the Cap Boujdour Area, Aaiun Basin, NW Africa. *Marine and Petroleum Geology* **27**, 435–441.

DEPERET, C. 1912. Sur l'âge des couches du Rio de Oro. *Comptes Rendus de l'Académie des Sciences* **13**, 123-124

ERHARDT, A.M, PÄLIKE H. & PAYTAN. A. 2013. High-resolution record of export production in the eastern equatorial Pacific across the Eocene-Oligocene transition and relationships to global climatic records. *Paleoceanography*, published online 25 March 2013.doi:10.1029/2012PA002347.

FEJFAR, O. 1987. Oligocene rodents from Zallah Oasis, Libya. *Münchner Geowissenschaftliche Abhandlungen* A10, 265–268.

FRONT Y SAGUE, N. 1911. Les formations géologiques du Rio de Oro, Sahara espagnol. *Bulletin de la Société Géologique de France* **4**, 212-217

JOLEAUD, L. 1907. Note sur quelques dents de Poissons fossiles du Rio de Oro (Sahara occidental). *Bulletin de la Société Géologique de France* **7**, 514.

GINGERICH, P.H. 1993. Oligocene age of the Gebel Qatrani Formation, Fayum, Egypt. *Journal of Human Evolution* **24**, p. 207-218.

GRADSTEIN, F.M., OGG, J.G., SCHMITZ, M.D., & OGG, G.M., (eds.), 2012. The geologic time scale 2012. Amsterdam, Netherlands, Elsevier, 1144 p.

KATZ, M.E., MILLER, K.G., WRIGHT, J.D., WADE, B.S., BROWNING, J.V., CRAMER, B.S. & ROSENTHAL, Y. 2008. Stepwise transition from the Eocene greenhouse to the Oligocene icehouse. *Nature Geosciences* **1**, 329–334.

KIRSCHVINK, J.L. 1980. The least-square line and plane and analysis of palaeomagnetic data. *Geophysical Journal of the Royal Astronomical Society* **62**, 699-718.

KLINGELHOEFER, F., LABAILS, C., COSQUER, E., ROUZO, S., GÉLI, L., ASLANIAN, D., OLIVET, J.-L. , SAHABI, M., NOUZÉ, H. & UNTERNEHR, P. 2009. Crustal structure of the SW-Moroccan margin from wide-angle and reflection seismic data (the Dakhla experiment) Part A: Wide-angle seismic models. *Tectonophysics* **468**, p. 63–82.

KOLONIC, S., SINNINGHEDAMSTÉ, J.S., BÖTTCHER, M.E., KUYPERS, M.M.M., KUHNT, W., BECKMANN, B., SCHEEDER, G. & WAGNER, T. 2002. Geochemical characterization of Cenomanian/Turonian black shales from the Tarfaya Basin (SW Morocco). *Journal of Petroleum Geology* **25**, 325-350.

LEAR, C.H., BAILEY, T.R., PEARSON, P.N., COXALL, H.K. & ROSENTHAL, Y. 2008. Cooling and ice growth across the Eocene-Oligocene transition. *Geology* **36,** 251–254.

LECOINTRE, G. 1962. Sur la géologie de la presqu'ile de villa Cisneron, Rio de Oro. *Comptes Rendus de l'Académie des Sciences* **254,** 1121-1122.

LECOINTRE, G. 1966. Néogène et Quaternaire du Rio de Oro (Maroc Espagnol). *Comptes Rendus de l'Académie des Sciences* **10**, 404-405.

LIU, Z., TUO, S., ZHAO, Q., CHENG, X. & HUANG, W. 2004. Deep-water earliest Oligocene Glacial Maximum (EOGM) in South Atlantic. *Chinese Science Bulletin* **49**, 2190-2197.

LOWRIE, W. 1990. Identification of ferrimagnetic minerals in rock by coercivity and unblocking temperature properties. *Geophysical Research Letters*, **17**, 159–162.

MARIVAUX, L., ADNET, S., BENAMMI, M., TABUCE, R., & BENAMMI, M., 2017. Anomaluroid rodents from the earliest Oligocene of Dakhla, Morocco, reveal the long-lived and morphologically conservative pattern of the Anomaluridae and Nonanomaluridae during the Tertiary in Africa. *Journal of Systematic Palaeontology*, published online 10 August 2016, doi:10.1080/14772019.2016.1206977.

MARIVAUX, L., ADNET, S., BENAMMI, M., TABUCE, R., YANS, Y., & BENAMMI, M., in press. Earliest Oligocene hystricognathous rodents from the Atlantic margin of Northwestern Saharan Africa (Dakhla, Morocco): systematic, paleobiogeographical and paleoenvironmental implications. *Journal of Vertebrate Paleontology.*

MILLER, K.G., WRIGHT, J.D. & FAIRBANKS, R.G. 1991. Unlocking the ice house: Oligocene-Miocene oxygen isotopes, eustasy and margin erosion. *Journal of Geophysical Research* **96**, 6829-6848.

ORTLIEB, L. 1975. Recherches sur les formations plio-quaternaire du littoral Ouest Saharien (28°30'-20°40'). PhD thesis, Pierre et Marie-Curie University, Paris VI - Trav. et Doc. ORSTOM, **48**, 267p.

PREMOLI-SILVA, I. & JENKINS, D.G. 1993. Decision on the Eocene-Oligocene boundary stratotype. *Episodes* **16**, 379-382.

RANKE, U., VON RAAD, U. & WISSMANN, G. 1982. Stratigraphy, facies, and tectonic development of on- and offshore Aaiun-Tarfaya Basin a review. In Geology of the North West African Continental Margin (ed U. Von Raad), pp 86–104. Springer-Verlag.

RASMUSSEN, D.T. & GUTIÉRREZ, M. 2010. Hyracoidea. In the Cenozoic Mammals of Africa (eds L.Werdlin & W.J. Sanders), pp.123-146. University of California Press, Berkeley.

RATSCHILLER, L.K. 1967. Sahara, correlazioni geologico-litostratigrapfiche fra Sahara Centrale ed Occidentale. *Mem. Mus. Tridentino Sc. Nat.*, **16**, 55-190.

RJIMATI, E., ZEMMOURI, A., BENLAKHDIM, A., AMZAEHOU, M., ESSALMANI, B., MUSTAPHI, H., HAIMOUK, M. & HAMIDI, F. 2008. Carte Géologique du Maroc. Ad-Dakhla, 1/100 000. *Notes et Mémoires Service Géologique du Maroc*, 487

SADDIQI, O., RJIMATI, E., MICHARD, A., SOULAIMANI, A. & OUANAIMI, H. 2015. Recommended Geoheritage Trails in Southern Morocco: A 3 Ga Record Between the Sahara Desert and the Atlantic Ocean. In From Geoheritage to Geoparks, Case Studies from Africa and Beyond (eds E. Errami, B. Margaret & S. Vic), pp. 91-108. Springer.

SACHSE, V.F., LITTKE, R., HEIM, S., KLUTH, O., SCHOBER, J., BOUTIB, L., JABOUR, H., PERSSEN, F. & SINDERN, S., 2011. Petroleum source rocks of the Tarfaya Basin and adjacent areas, Morocco. *Organic Geochemistry* **42**, 209-227.

SACHSE, V.F., HEIM, S., JABOUR, H., KLUTH, O., SCHÜMANN, T., AQUIT, M. & LITTKE, R. 2014. Organic geochemical characterization of Santonian to Early Campanian organic matter-rich marls (Sondage No. 1 cores) as related to OAE3 from the Tarfaya Basin, Morocco. *Marine and Petroleum Geology* **56**, 290-304.

SALLAM, H.M., SEIFFERT, E.R. & SIMONS, E.L. 2011. Craniodental morphology and systematics of a new family of hystricognathous rodents (Gaudeamuridae) from the Late Eocene and Early Oligocene of Egypt. *PLoS ONE* **6**, e16525eol.

SALLAM, H.M. &SEIFFERT, E.R. 2016. New phiomorph rodents from the latest Eocene of Egypt, and the impact of Bayesian "clock" based phylogenetic methods on estimates of basal hystricognath relationships and biochronology. *PeerJ* **4**, e1717.

SARKAR, A., SARANGIB, S., EBIHARAC, M., BHATTACHARYAD, S.K. & RAYE, A.K. 2003.Carbonate geochemistry across the Eocene/Oligocene boundary of Kutch, western India: implications to oceanic O2-poor condition and foraminiferal extinction: *Chemical Geology* **201**, 281–293.

SEIFFERT, E.R. 2006. Revised age estimates for the later Paleogene mammal faunas of Egypt and Oman. *Proceedings of the National Academy of Sciences of the USA* **103**, 5000–5005.

SEIFFERT, E.R. 2012. Early primate evolution in Afro-Arabia. *Evolutionary Anthropology* **21**, 239–253.

SIMONS, E.L. & RASMUSSEN, D.T. 1996. Skull of *Catopithecus browni*, an early Tertiary catarrhine. *American Journal of Physical Anthropology* **100**, 261–292.

SIMONS, E.L., HOLROYD, P.A & BOWN, T.M. 1991. Early Tertiary elephant shrews from Egypt and the origin of the Macroscelidea. *Proceedings of the National Academy of Sciences of the USA* **88**, 9734–9737.

STORME, J.-Y., DEVLEESCHOUWER, X., SCHNYDER, J., CAMBIER, G., BACETA, J.I., PUJALTE, V., IACUMIN, P. & YANS, J. 2012. Paleocene/Eocene boundary section at Zumaia (Basque-Catabric Basin) revisited: new insights from high resolution magnetic susceptibility and carbon isotope chemostratigraphy on organic matter ($\delta^{13}C_{org}$). *Terra Nova* **24**, 310-317.

STRECHIE, C., ANDRE, F., JELINOWSKA, A., TUCHOLKA, P., GUICHARD, F., LERICOLAIS, G. & PANIN, N. 2002. Magnetic minerals as indicators of major environmental change in Holocene Black Sea sediments: preliminary results. *Physics Chemistry Earth* **27**, 1363–1370.

TRAMOY, R., SALPIN, M., SCHNYDER, J., PERSON, A., SEBILO, M., YANS, J., VAURY, V., FOZZANI, J. & BAUER, H. 2016. Stepwise paleoclimate change across the Eocene-Oligocene transition recorded in continental NW Europe by mineralogical assemblages and $\delta^{15}N_{org}$ (Rennes Basin, France). *Terra Nova* **28**, 212–220

TUDRYN, A. & TUCHOLKA, P. 2004. Magnetic monitoring of thermal alteration for natural pyrite and greigite. *Acta Geophysica Polonica* **52**, 509–520.

UNDERWOOD, C.J., KING, C. & STEURBAUT, E. 2013. Eocene initiation of Nile drainage due to East African uplift. *Palaeogeography, Palaeoclimatology, Palaeoecology* **392**, 138–145.

VANDENBERGHE, N., HILGEN, F.J. & SPEIJER, R. 2012. The Paleogene Period. In The Geological Time Scale. (eds F.M. Gradstein, J.G. Ogg, M.D. Schmitz, G.M. Ogg). 2012. Elsevier Science Ltd, Oxford **2**, 855-921.

YANS, J., GERARDS, T., GERRIENNE, P., SPAGNA, P., DEJAX, J., SCHNYDER, J., STORME, J.-Y. & KEPPENS, E. 2010. Carbon-isotope of fossil wood and dispersed organic matter from the terrestrial Wealden facies of Hautrage (Mons basin, Belgium). *Palaeogeography, Palaeoclimatology, Palaeoecology* **291**, 85-105.

WOOD, A.E. 1968. Part II: The African Oligocene Rodentia; in Early Cenozoic Mammalian Faunas Fayum Province, Egypt (ed J.E. Remington). pp. 23–105. Peabody Museum of Natural History Yale University, New Haven, Connecticut.

ZHIFEI, L., SHOUTING, T., QUANHONG Z., XINRONG, C. & WEI, H. 2004. Deep-water Earliest Oligocene Glacial Maximum (EOGM) in South Atlantic. Chinese Science Bulletin **49**, 2190-2197.

ZIJDERVELD, J. D. A. 1967. AC demagnetization rocks-Analyses of results. In Methods in paleomagnetism (eds D. W. Collinson, K.M. Creer & S.K. Runcorn), p. 254–286. Amsterdam, Netherlands, Elsevier Scientific.

ZOUHRI, S., GINGERICH, P.D., EL BOUDALI, N., SEBTI, S., NOUBHANI, A., RAHALI, M. & MESLOUH, S. 2014. New marine mammal faunas (Cetacea and Sirenia) and sea level change in the Samlat Formation, upper Eocene, near Ad-Dakhla in southwestern Morocco. *Comptes Rendus Palevol* **13**, 599-610.

Figures captions

Figure 1: Geographic location of the Dakhla peninsula, south of Morocco. (a), map of Morocco with principal towns; (b), location of the geological sections studied (stars). 1: Garitas, 2: Porto Rico, 3: El Argoub. The black circles denote the outcrops of interest along the Atlantic Ocean coast.

Figure 2: Stratigraphic section of the Garitas sedimentological sequence. U1-U5 refers to the unit and the number on the right of the column represents the lithofacies.

Figure 3: Field photographs showing: (a) a general view of the lower part of the Garitas section, horizontal heterolithic stratification; (b) a detail of A, showing blackish (A1) rich in organic matter levels; (c) a phosphorite rich organic matter with shark teeth (fossil-bearing level A1); (e) the beige marl and siliceous limestone with Neptunian dykes in (f).

Figure 4: Field photographs showing: (a) an example of coprolite level; (b) a succession of gray limestone bar and beige sandy calcareous marl (lithofacies 3 in figure 2), black to brown or dark siliceous limestone with coprolites at its base (lithofacies 4), yellowish sandy marl rich in vertebrate fossil, fossil-bearing level B1 (lithofacies 5); (c) a whitish marl with lenticular brown siliceous limestone (lithofacies 6).

Figure 5: Garitas section. (a) lithofacies 6 forms the prominent ledge; (b) overlaying muddy brown yellow sandstone corresponding to fossil-bearing level B2 (lithofacies 7).

Figure 6: Field photographs showing the top of the Garitas section with lithofacies 9, 10 and 11.

Figure 7: Porto Rico section. (a) general view of the lower part of the section with the fossil-bearing levels B1 and B2; (b) exposure of the Unit U3 corresponding to the lithofacies 3, which consists of a thick multicolor sandy marl series interstratified by sandstone with limestone concretions (we can see the position of fossil-bearing levels C1 and C2); (c)

photograph showing the abundant selachian teeth of the B2 level; (d) landmark level of gastropods and oysters coquina.

Figure 8: field photographs and measured section of North Porto Rico and El Argoub areas. (a) section located 2 km north of El Argoub village, (b, c) sections is about 6 km north of Portorico. See the landmark level consisting of gastropod and oyster coquina at the lower part of U4.

Figure 9: Outline correlation between cross sections from Garitas to El Argoub.

Figure 10: Porto Rico section and position of paleomagnetic sampling and the NRM intensities plotted against lithostratigraphic position (right curve). Note the position of the fossil-bearing B1, B2, C1 and C2.

Figure 11: Paleomagnetic analysis: (a) acquisition of isothermal remanent magnetization (IRM) (normalized values) curves of same samples, with most of the magnetization acquired below 200 mT and saturation achieved at 300 mT; (b, c) stepwise thermal demagnetization of the IRM components; (d) thermomagnetic curve of sample, where magnetic iron sulphides where suspected to be present in the samples.

Figure 12: Demagnetization plots of the samples. The solid (open) symbols represent horizontal (vertical) projections, respectively. (a) at 10 mT, the magnetization intensity fall below the noise level of the magnetometer; (b) example of samples with erratic direction; (c) example of samples with normal polarity from the site situated 2m above the C1 fossil-bearing level; (d) equal area projection and Fisher statistics of the reliable characteristic remanent magnetization (ChRM) direction. The 95% confidence ellipse for the normal (solid star) mean directions is indicated (inclination=44.6°, declination=324.4°). Gray star is the geocentric axial dipole of the Porto Rico latitude.

Figure 13: Carbon isotope values (‰ VPDB) of the Porto Rico and El Argoub sections, compared to δ^{13}Ccurves around the Eocene-Oligocene transition in ODP Site 1218 (Erhardt et al., 2013) and reference δ^{13}C composite curve (Cramer et al., 2009 modified by Vandenberghe et al., 2012). EOT=Eocene-Oligocene Transition; U1 to U5 refer to the lithological units defined in the text. B1, B2, C1 and C2 are fossil-bearing levels.

Table 1: Sample labels, $CaCO_3$ content (%) and $\delta^{13}C_{org}$ values (‰, VPDB); N.A.= not analyzed.

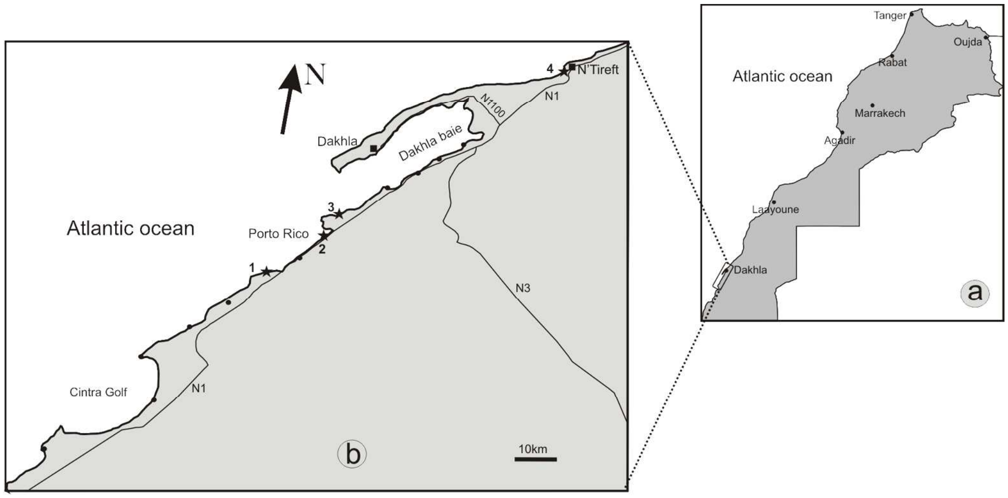

Geographic location of the Dakhla peninsula, south of Morocco. (a), map of Morocco with principal towns; (b), location of the geological sections studied (stars). 1: Garitas, 2: Porto Rico, 3: El Argoub. The black circles denote the outcrops of interest along the Atlantic Ocean coast.

169x83mm (300 x 300 DPI)

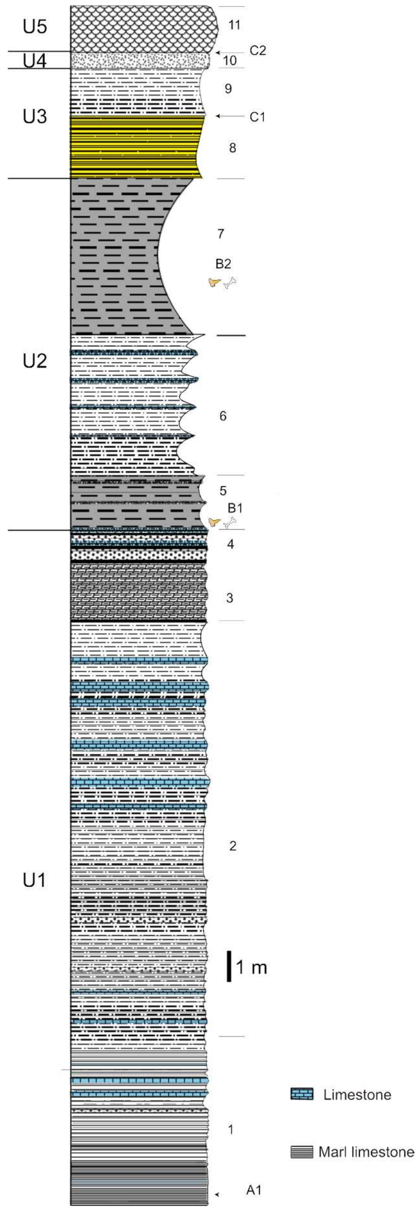

Stratigraphic section of the Garitas sedimentological sequence. U1-U5 refers to the unit and the number on the right of the column represents the lithofacies.

79x234mm (300 x 300 DPI)

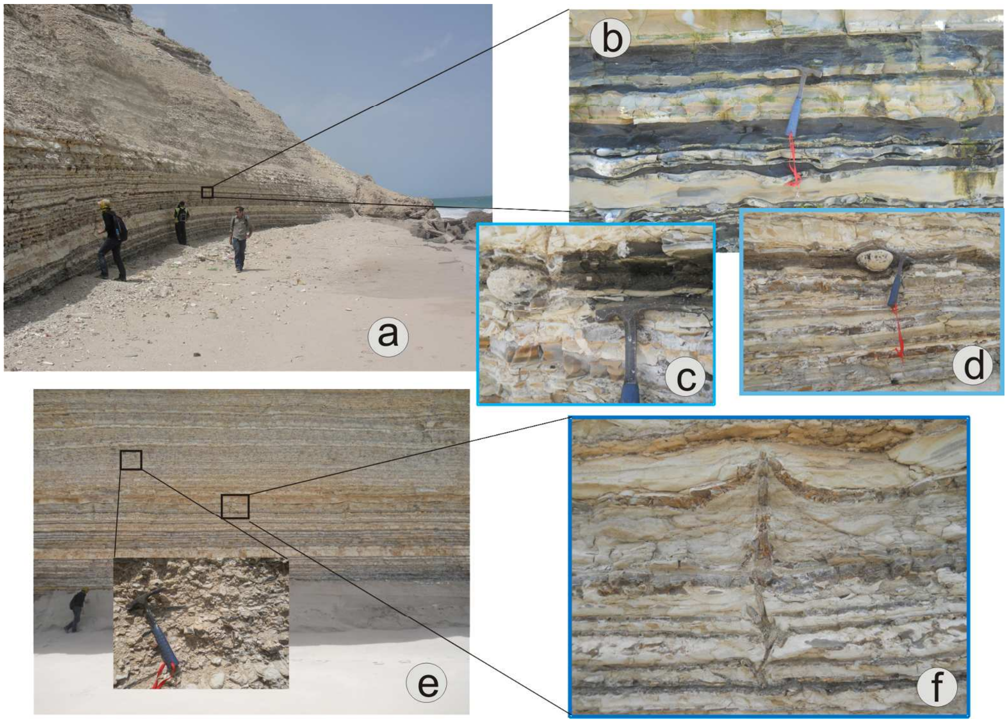

Field photographs showing: (a) a general view of the lower part of the Garitas section, horizontal heterolithic stratification; (b) a detail of A, showing blackish (A1) rich in organic matter levels; (c) a phosphorite rich organic matter with shark teeth (fossil-bearing level A1); (e) the beige marl and siliceous limestone with Neptunian dykes in (f).

169x121mm (300 x 300 DPI)

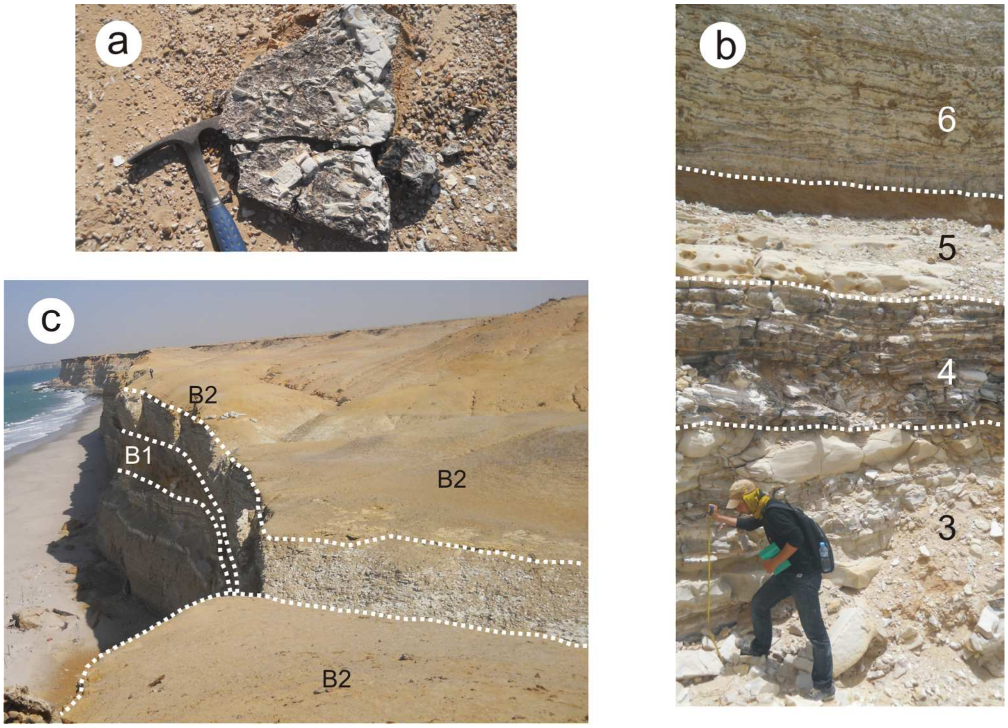

Field photographs showing: (a) an example of coprolite level; (b) a succession of gray limestone bar and beige sandy calcareous marl (lithofacies 3 in figure 2), black to brown or dark siliceous limestone with coprolites at its base (lithofacies 4), yellowish sandy marl rich in vertebrate fossil, fossil-bearing level B1 (lithofacies 5); (c) a whitish marl with lenticular brown siliceous limestone (lithofacies 6).

170x122mm (300 x 300 DPI)

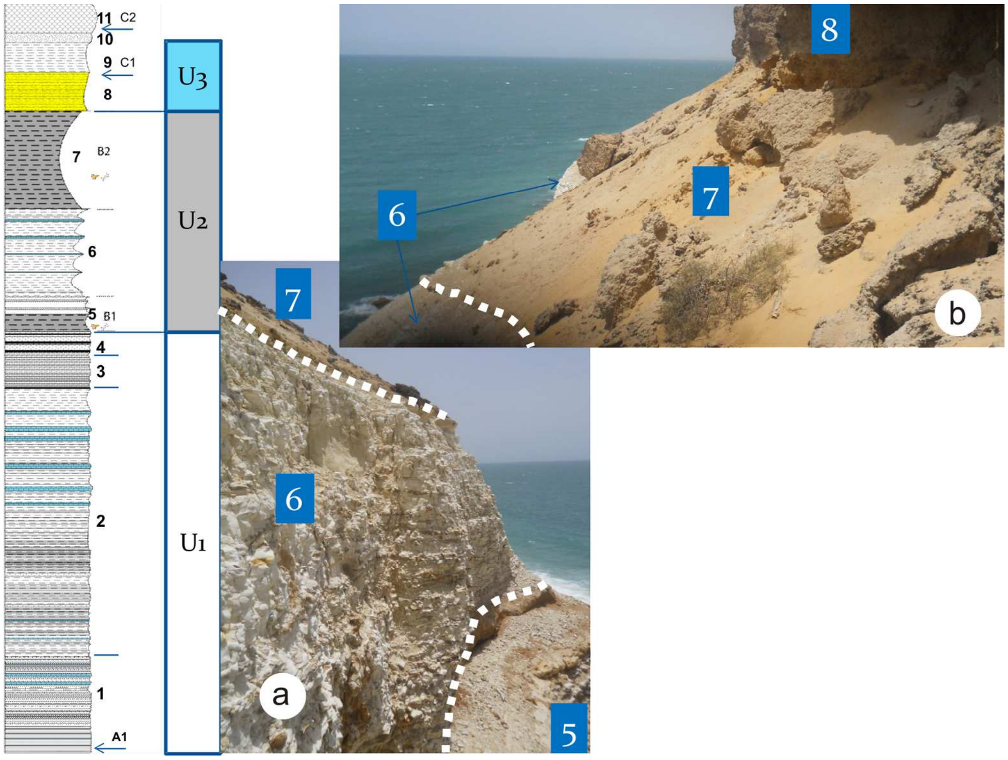

Garitas section. (a) lithofacies 6 forms the prominent ledge; (b) overlaying muddy brown yellow sandstone corresponding to fossil-bearing level B2 (lithofacies 7).

173x130mm (300 x 300 DPI)

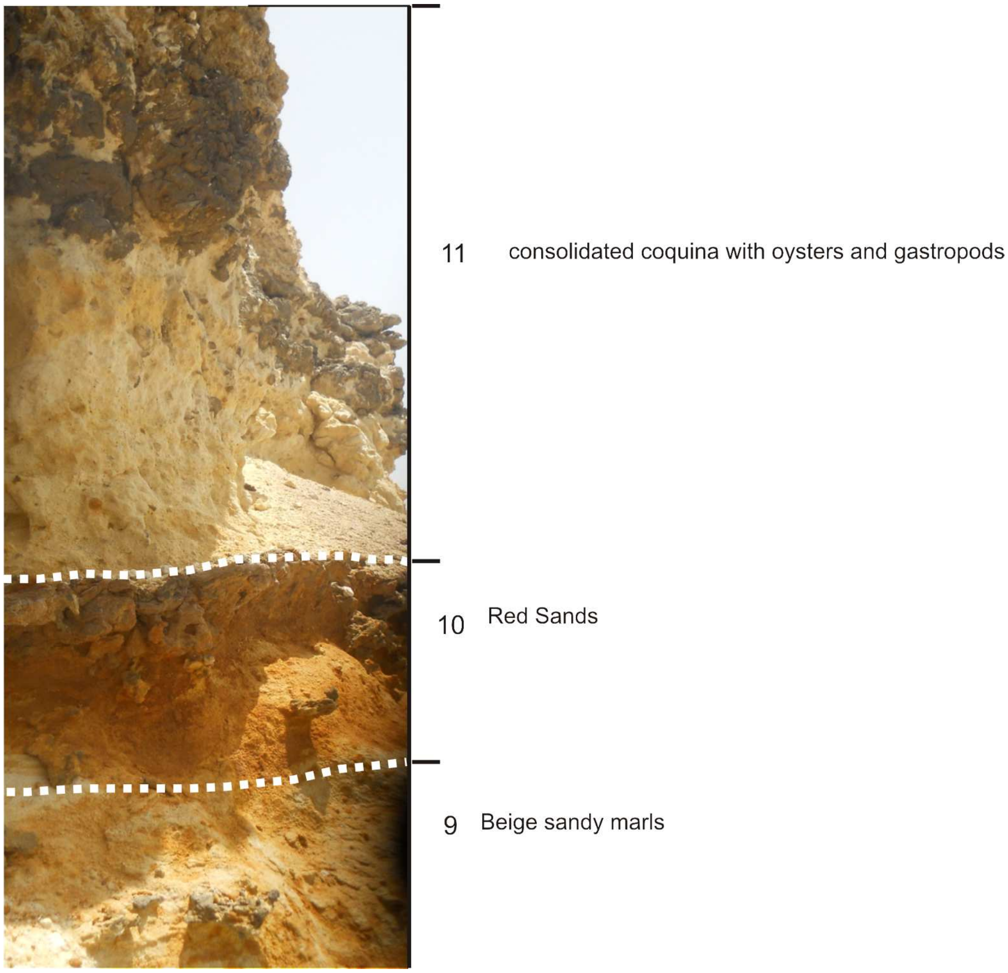

Field photographs showing the top of the Garitas section with lithofacies 9, 10 and 11.

169x163mm (300 x 300 DPI)

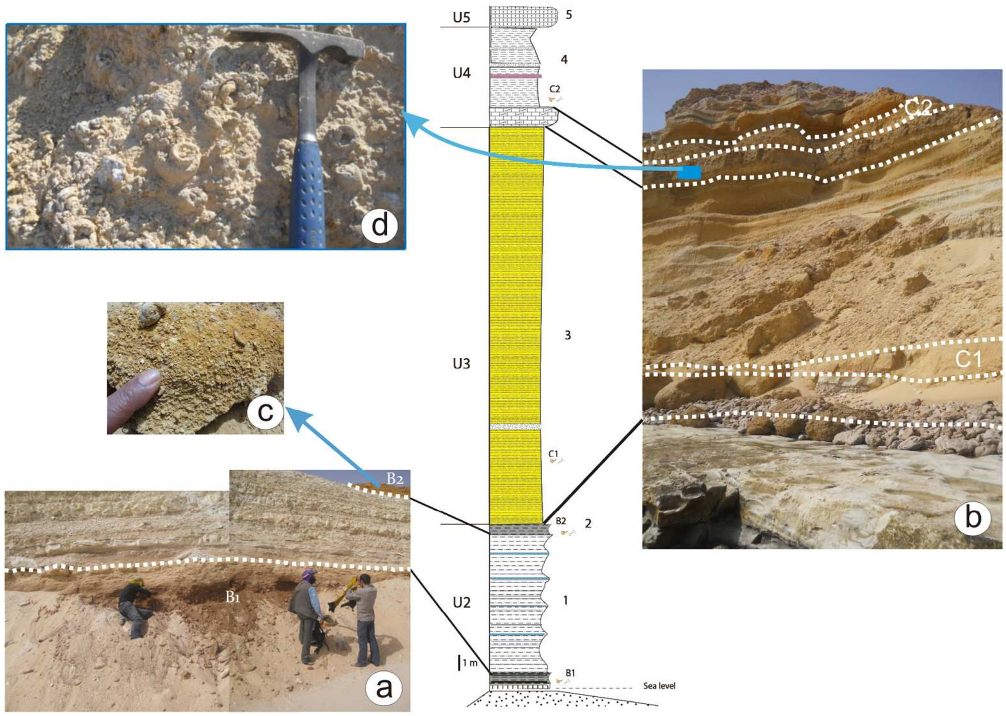

Porto Rico section. (a) general view of the lower part of the section with the fossil-bearing levels B1 and B2; (b) exposure of the Unit U3 corresponding to the lithofacies 3, which consists of a thick multicolor sandy marl series interstratified by sandstone with limestone concretions (we can see the position of fossil-bearing levels C1 and C2); (c) photograph showing the abundant selachian teeth of the B2 level; (d) landmark level of gastropods and oysters coquina.

170x120mm (300 x 300 DPI)

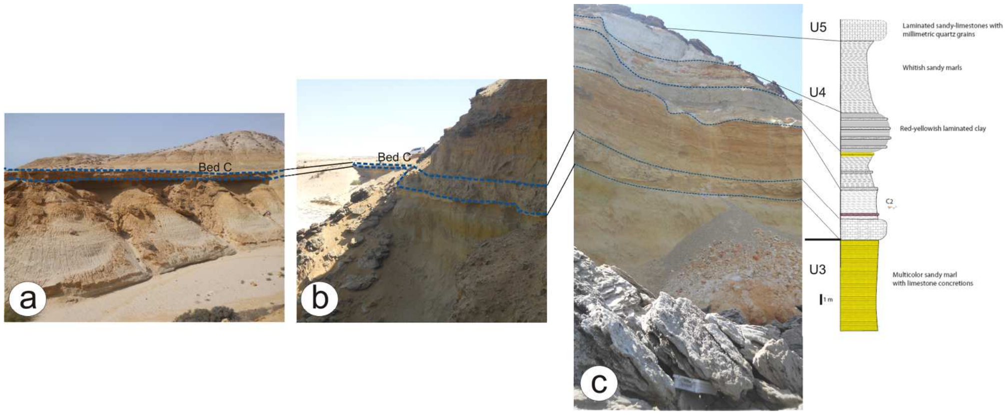

field photographs and measured section of North Porto Rico and El Argoub areas. (a) section located 2 km north of El Argoub village, (b, c) sections is about 6 km north of Portorico. See the landmark level consisting of gastropod and oyster coquina at the lower part of U4.

167x68mm (300 x 300 DPI)

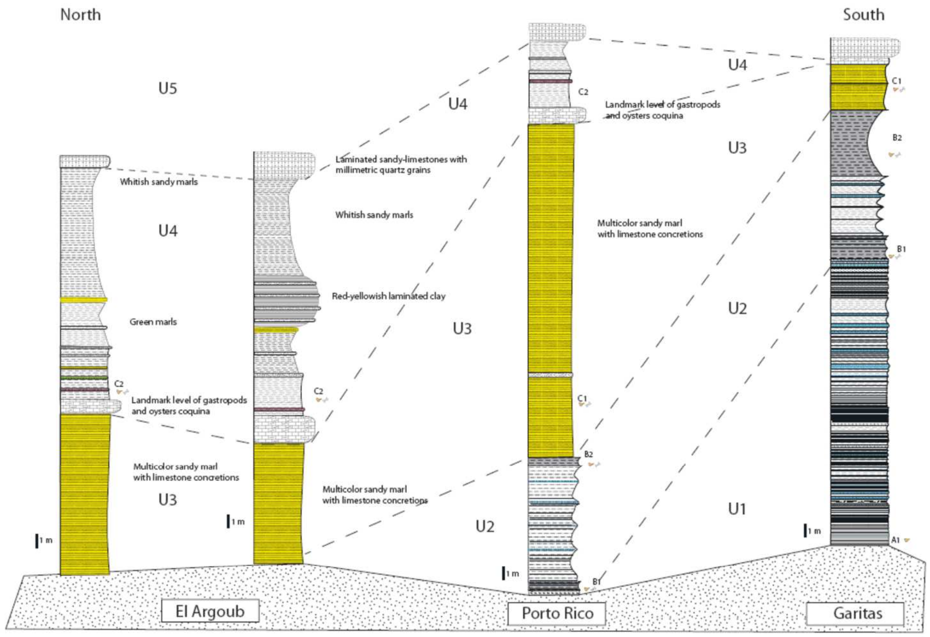

Outline correlation between cross sections from Garitas to El Argoub.

170x119mm (300 x 300 DPI)

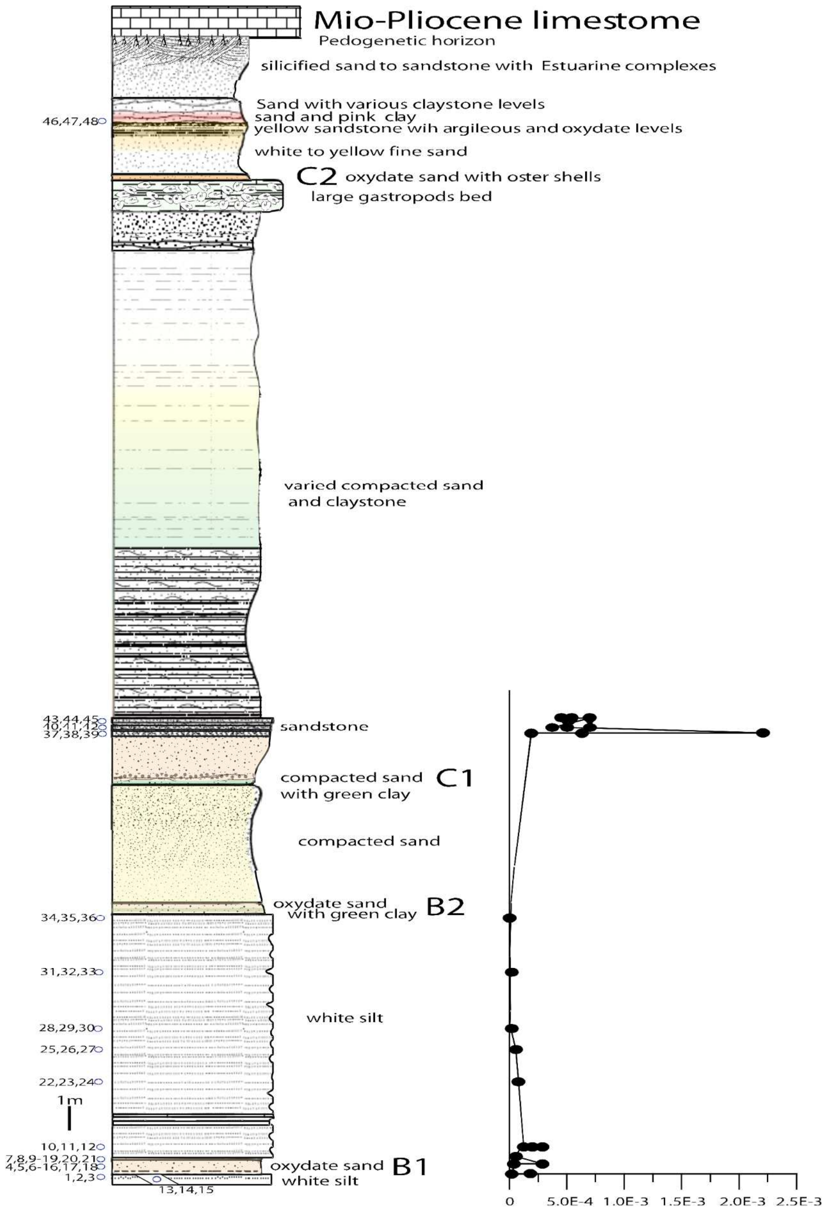

Porto Rico section and position of paleomagnetic sampling and the NRM intensities plotted against lithostratigraphic position (right curve). Note the position of the fossil-bearing B1, B2, C1 and C2.

158x232mm (300 x 300 DPI)

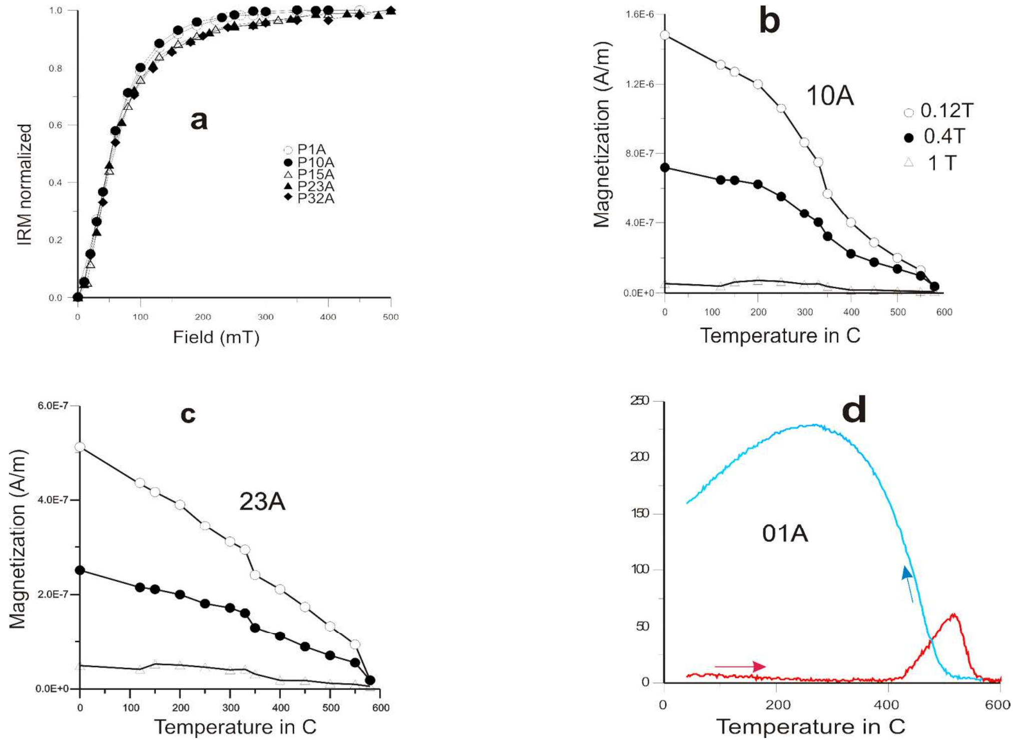

Paleomagnetic analysis: (a) acquisition of isothermal remanent magnetization (IRM) (normalized values) curves of same samples, with most of the magnetization acquired below 200 mT and saturation achieved at 300 mT; (b, c) stepwise thermal demagnetization of the IRM components; (d) thermomagnetic curve of sample, where magnetic iron sulphides where suspected to be present in the samples.

170x124mm (300 x 300 DPI)

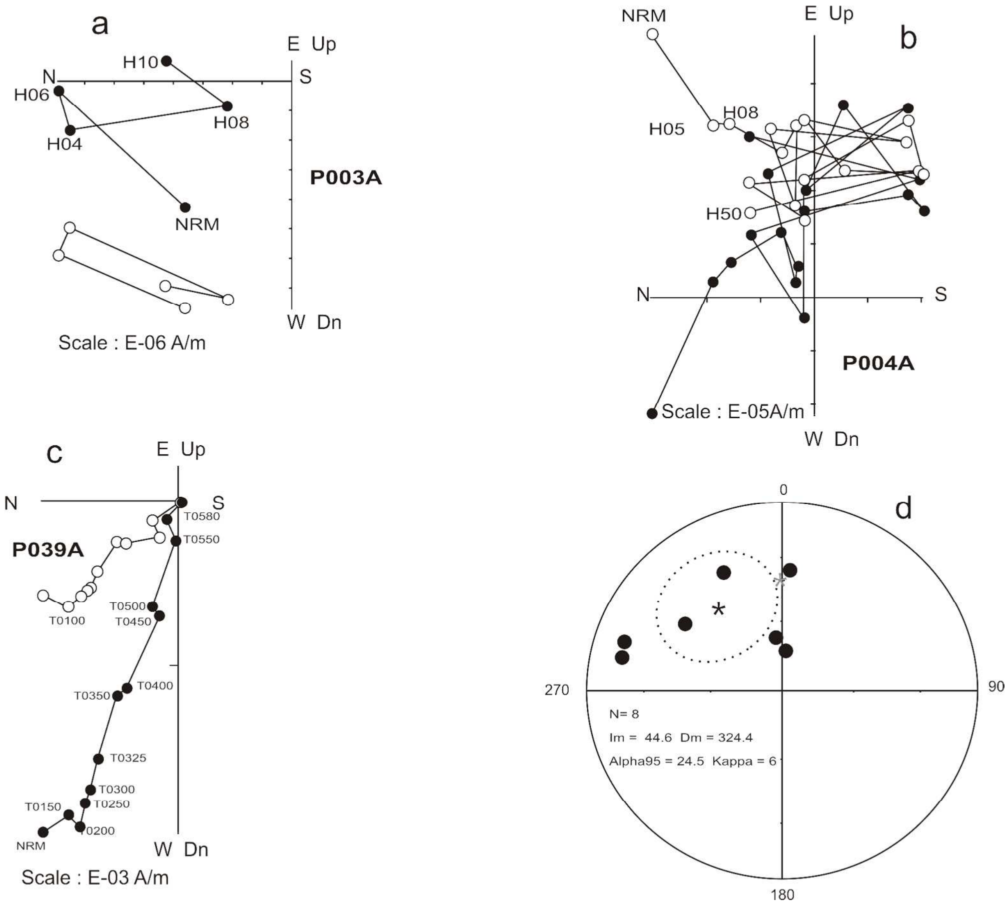

Demagnetization plots of the samples. The solid (open) symbols represent horizontal (vertical) projections, respectively. (a) at 10 mT, the magnetization intensity fall below the noise level of the magnetometer; (b) example of samples with erratic direction; (c) example of samples with normal polarity from the site situated 2m above the C1 fossil-bearing level; (d) equal area projection and Fisher statistics of the reliable characteristic remanent magnetization (ChRM) direction. The 95% confidence ellipse for the normal (solid star) mean directions is indicated (inclination=44.6°, declination=324.4°). Gray star is the geocentric axial dipole of the Porto Rico latitude.

170x152mm (300 x 300 DPI)

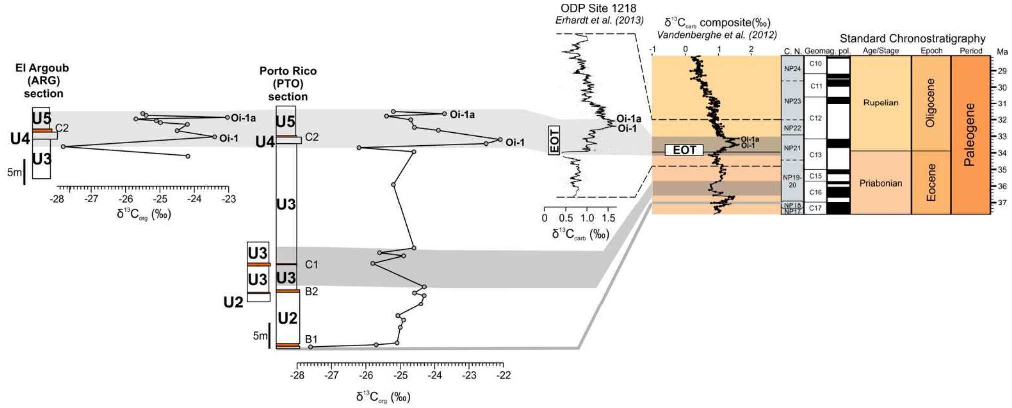

Carbon isotope values (‰ VPDB) of the Porto Rico and El Argoub sections, compared to δ13Ccurves around the Eocene-Oligocene transition in ODP Site 1218 (Erhardt et al., 2013) and reference δ13C composite curve (Cramer et al., 2009 modified by Vandenberghe et al., 2012). EOT=Eocene-Oligocene Transition; U1 to U5 refer to the lithological units defined in the text. B1, B2, C1 and C2 are fossil-bearing levels.

170x68mm (300 x 300 DPI)

section	label	$CaCO_3$ (%)	$\delta^{13}C_{org}$ (‰ VPDB)
Porto Rico section	PTO15-18	0.0	-25.2
	PTO15-17	0.0	-23.7
	PTO15-16	0.0	-25.4
	PTO15-15	0.0	-24.7
	PTO15-14	0.0	-24.6
	PTO15-13	0.0	-23.9
	PTO15-11	55.1	-22.1
	PTO15-10	1.0	-22.5
	PTO15-9	0.6	-26.2
	PTO15-8	5.0	-24.6
	PTO15-7	0.0	-25.2
	PTO15-5	0.0	-24.6
	PTO-41	2.0	-25.6
	PTO15-4	0.0	-25.0
	PTO15-3	0.0	-25.8
	PTO15-2	1.2	-24.3
	PTO-34	76.0	-24.6
	PTO15-1	76.9	-24.3
	PTO-32B	1.0	-24.4
	PTO-30B	1.0	-25.1
	PTO-26B	1.0	-24.9
	PTO-22B	2.0	-25.0
	PTO-21B	59.0	-25.1
	PTO-16B	60.0	-25.7
	PTO-2	43.0	-27.6
El Argoub section	ARG15-12	0.0	-25.5
	ARG15-11	0.0	-25.4
	ARG15-10	1.4	-23.0
	ARG15-9	1.3	-25.7
	ARG15-8	0.0	-25.1
	ARG15-7	1.0	-25.0
	ARG15-6	3.2	-24.2
	ARG15-4	45.3	-24.5
	ARG15-3	28.7	-23.4
	ARG15-2	0.0	-27.8
	ARG15-1	0.5	-24.2
Not analyzed (TOC too low)	PTO15-12	41.2	TOC too low
	PTO15-6	0.0	TOC too low
	ARG15-5	N.A.	TOC too low
	PTO-43	3.0	TOC too low
	PTO-19	N.A.	TOC too low
	PTO-11	19.0	TOC too low
	PTO-5	N.A.	TOC too low

Sample labels, CaCO3 content (%) and δ13Corg values (‰, VPDB); N.A.= not analyzed.

210x297mm (200 x 200 DPI)